

Timing irregularities of PSR J1705–1906

Y. L. Liu^{1,2} • J. P. Yuan^{†,2,3,4} • J. B. Wang^{2,4} •
X. W. Liu¹ • N. Wang^{2,3,4} • R. Yuen^{2,3}

Abstract

Timing analysis of PSR J1705–1906 using data from Nanshan 25-m and Parkes 64-m radio telescopes, which span over fourteen years, shows that the pulsar exhibits significant proper motion, and rotation instability. We updated the astrometry parameters and the spin parameters of the pulsar. In order to minimize the effect of timing irregularities on measuring its position, we employ the Cholesky method to analyse the timing noise. We obtain the proper motion of $-77(3)$ mas yr⁻¹ in right ascension and $-38(29)$ mas yr⁻¹ in declination. The power spectrum of timing noise is analyzed for the first time, which gives the spectral exponent $\alpha = -5.2$ for the power-law model indicating that the fluctuations in spin frequency and spin-down rate dominate the red noise. We detect two small glitches from this pulsar with fractional jump in spin frequency of $\Delta\nu/\nu \sim 2.9 \times 10^{-10}$ around MJD 55199 and $\Delta\nu/\nu \sim 2.7 \times 10^{-10}$ around MJD 55953. Investigations of pulse profile at different time segments suggest no significant changes in the pulse profiles around the two glitches.

Keywords stars: neutron — pulsars: general — pulsars: individual(PSR J1705–1906)

1 Introduction

Discovered in the second Molonglo pulsar survey (Manchester et al. 1978), PSR J1705–1906 is a radio and γ -ray pulsar with a rotation period of 0.299 s and period derivative of $4.1 \times 10^{-15} \text{ s s}^{-1}$. The pulsar has a characteristic age $\tau_c \sim 1.16 \times 10^6$ yr, and a spin-down energy loss rate of $6.11 \times 10^{33} \text{ erg s}^{-1}$. Assuming magnetic dipolar braking, PSR J1705–1906 has a surface dipole magnetic field $B_s \sim 1.12 \times 10^{12} \text{ G}$. High-energy pulsed emission was also detected from the pulsar using the Fermi Gamma-ray telescope, which revealed a γ ray luminosity of $0.25(8) \times 10^{33} \text{ erg s}^{-1}$ with efficiency of 4%, and a spectral index of 2.3(2) (Hou et al. 2014). The pulse profile exhibits a clear single peak between 0.1 - 300 GeV, which can be well-fitted with a Lorentz function. Note that the Fermi telescope has no detection of cut-off energy. X-ray counterpart was not confirmed with the XMM-Newton 8 ks observation between 0.3 and several keV bands (Hou et al. 2014).

It has long been recognized that pulsars are high-velocity objects with space velocities up to an order of magnitude larger than that of their progenitors (Gunn and Ostriker 1970; Hobbs et al. 2005). A natural explanation for such high velocities is that supernova explosions are non-homogeneous resulting in kicks to the nascent pulsars (Lai and Qian 1998; Lai et al. 2001; Ng and Romani 2006). Pulsar velocities are determined by measuring their proper motions and distances. For radio pulsars with high intensity, their positions and proper motions can be precisely determined using Very Long Baseline Interferometry (VLBI) (Briskin et al. 2002, 2003; Deller et al. 2016). In recent years, the proper motion of some

Y. L. Liu

J. P. Yuan

J. B. Wang

X. W. Liu

N. Wang

R. Yuen

[†] E-mail: yuanjp@xao.ac.cn

¹School of Physics, China West Normal University, Nanchong, Sichuan, China, 637002

²Xinjiang Astronomical Observatory, CAS, 150 Science 1-Street, Urumqi, Xinjiang, China, 830011

³Key Laboratory of Radio Astronomy, Chinese Academy of Sciences, Nanjing 210008, China

⁴Xinjiang Key Laboratory of Radio Astrophysics, 150 Science 1-Street, Urumqi, Xinjiang, 830011, China

weak pulsars have also been obtained by VLBI. For example, Yan et al. (2013) measured the astrometric parameters of PSR B1257+12 in the three-planet pulsar system using Very Long Baseline Array (VLBA) and European VLBI Network (EVN), and Du et al. (2014) acquired the parallax and proper motion for the weak millisecond pulsar PSR J0218+4232 with EVN at 1.6 GHz. In addition, astrometric parameters can be determined by pulsar timing observations with data that spans over several years (Manchester et al. 1974; Hobbs et al. 2005; Li et al. 2016). PSR J1705–1906 is a nearby pulsar with an estimated distance of 0.9(1) kpc based on the Galactic free electrons density model (NE2001), but its parallax is not reported. Previous studies of PSR J1705–1906 reported its positions close to the ecliptic plane with ecliptic longitude of 257.135499° , ecliptic latitude of 3.72327° , right ascension of 17:05:36.099 and declination of $-19:06:38.6$ (Hobbs et al. 2004). The proper motion of the pulsar in ecliptic coordinates is presented with $\mu_\lambda = -66(5) \text{ mas yr}^{-1}$ and $\mu_\beta = -123(83) \text{ mas yr}^{-1}$, as well as in equatorial with $\mu_\alpha = -78(9) \text{ mas yr}^{-1}$ and $\mu_\delta = -116(82) \text{ mas yr}^{-1}$ (Hobbs et al. 2004).

Pulsar timing is a high-precision discipline, which allows the observed pulse Time of Arrivals (ToAs) to be compared with a model of the pulsar’s astrometric, orbital and rotational, parameters (Hobbs et al. 2006). The difference between the predicted arrival time and the actual arrival time is known as the pulsar’s timing residual. Long-term timing observations reveal two main sources of timing irregularities, namely the timing noise and glitch, where the latter exhibits as a sudden speed-up in the spin-down rate of a pulsar. Timing noise is a continuous behavior with low frequency quasi-sine structure (called red noise) over time scale of months to years, which is commonly caused by irregularities in the intrinsic pulsar rotation. For most observed glitches, the increase in spin-frequency, ν , ranges from 10^{-9} Hz to 10^{-5} Hz (Yuan et al. 2010; Espinoza et al. 2011; Yu et al. 2013). For PSR J1705–1906, a glitch with $\Delta\nu/\nu \sim 0.4 \times 10^{-9}$ was detected in 1992 (Espinoza et al. 2011). After a glitch, there are often exponential recovery in spin-frequency (ν) and decay of the frequency derivative ($\dot{\nu}$) back to their pre-glitch values. This relaxation can vary significantly from pulsar to pulsar, and even from glitch to glitch in the same pulsar (D’Alessandro 1996). A more complete understanding of pulsar timing irregularities will lead to many important results, such as explaining the cause of timing noise and glitches, which may also allow correlations to form between these phenomena and hence provide unique insights into the interior structure of neutron stars.

This paper is organized as follows. We describe the observing system and the data reduction of PSR J1705–1906 in Section 2. In Section 3, we obtain the latest information on astrometric measurements for the pulsar. In Section 4, we present the analysis of red timing noise and describe the two glitches. In Section 5, we investigate whether there is any change in the pulse profile of PSR J1705–1906 associated these glitches. We discuss our results in Section 6.

2 Observations and data reduction

The Nanshan telescope is equipped with a dual-channel cryogenic receiver operating at frequency band centered at 1.54 GHz with a bandwidth of 0.32 GHz. Early observations, prior to 2010, were taken using an Analogue Filter-Bank (AFB) that has 128 2.5 MHz sub-channels for each of the two polarizations (Wang et al. 2001). Since January 2010, observations have been made using the Digital Filter-Bank (DFB) with 0.5 MHz bandwidth for each sub-channel where four Stokes parameters are collected from the two orthogonal polarizations. Data is folded on-line with sub-integration time of 1 min for the AFB and 30 s for the DFB, and then written to disk with 256 bins across the pulse profile for the AFB and 512 bins for the DFB. PSR J1705–1906 was observed roughly three times per month with 4 minutes each time at Nanshan. The observations at Parkes were carried out between April 2001 and Feb 2014 with a central observing frequency close to 1.37 GHz. Several observations of this pulsar were conducted with the 10-cm receiver which has a bandwidth of 1024 MHz centered at 3094 MHz. The raw data is acquired by using a suite of Parkes digital filter-bank systems (Hobbs et al. 2011) and all of the pulsar data was stored in the data archive¹ following the PSRFITS software (Hotan et al. 2004). The details for receivers, back-ends and the data set can be found in Table 1.

The PSRCHIVE analysis system is used to dispel radio-frequency interference, fold and de-disperse the multi-channel data to get effective pulse profiles (Hotan et al. 2004). The TEMPO2 software is then used to calculate the barycentric arrival time, form the timing residuals and carry out the weighted least-square fit (Hobbs et al. 2006; Edwards et al. 2006). The timing model for barycentric pulse phase, ϕ , as a function of time t , is,

$$\phi(t) = \phi_0 + \nu(t - t_0) + \frac{1}{2}\dot{\nu}(t - t_0)^2 + \frac{1}{6}\ddot{\nu}(t - t_0)^3, \quad (1)$$

¹<https://datanet.csiro.au/dap>

Table 1 Description of the observations showing the telescope, receiver, centre frequency and the bandwidth (BW). The last two columns are the number of ToAs and the MJD ranges over which the observations spanned.

Telescope	Receiver	Freq.(MHz)	BW(MHz)	Backend	No.of ToAs	MJD range
Nanshan	(non-)cryogenic	1540	320	AFB	510	51561–56717
Nanshan	cryogenic	1556	320	PDFB3	120	55239–56720
Parkes	MULTI	1374	288	AFB	12	52001–54009
Parkes	MULTI	1369	256	PDFBs	86	54303–56740
Parkes	1050CM	3094	1024	PDFBs	16	54305–56683

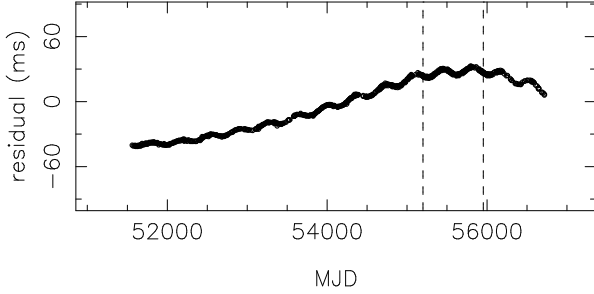


Fig. 1 The timing residuals for PSR J1705–1906 with respect to the ephemeris given by Hobbs et al. (2004).

where ϕ_0 is the phase at time t_0 , and ν , $\dot{\nu}$, $\ddot{\nu}$ represent the pulse frequency, frequency derivative and frequency second derivative, respectively. A glitch will result in an additional pulse phase that can be modeled by the equation:

$$\phi_g = \Delta\phi + \Delta\nu_p(t - t_g) + \frac{1}{2}\Delta\dot{\nu}_p(t - t_g)^2 + [1 - e^{-(t-t_g)/\tau_d}]\Delta\nu_d\tau_d, \quad (2)$$

where t_g is the glitch epoch and $\Delta\phi$ is an offset of pulse phase between the pre- and post-glitch data. The glitch event is characteristic with permanent increments in the spin frequency $\Delta\nu_p$ and first frequency derivative $\Delta\dot{\nu}_p$ and a transient frequency increment $\Delta\nu_d$ which decays exponentially with a time scale τ_d .

3 Astrometry of PSR J1705–1906

3.1 Position and proper motion

Figure 1 shows the timing residuals for PSR J1705–1906, which is obtained using the ephemeris (shown in Table 2) from the ATNF Pulsar Catalogue². The residuals appear to exhibit periodic oscillation on a time scale of one year owing to the proper motion.

Table 2 The ephemeris for PSR J1705–1906 (Hobbs et al. 2004).

NAME	PSR J1705–1906
RAJ (h:m:s)	17:05:36.099(3)
DECJ (° :′ :″)	−19:06:38.6(4)
DM (pc cm ^{−3})	22.907(3)
PEPOCH (MJD)	48733.00
POSEPOCH (MJD)	48733.00
ν (Hz)	3.344622243443(18)
$\dot{\nu}$ ($\times 10^{-15}$ Hz s ^{−1})	−46.28835(11)
$\ddot{\nu}$ ($\times 10^{-15}$ Hz s ^{−2})	0.334(15)
EPHVER	2
UNITS	TDB

Table 3 The positions of PSR J1705–1906 in equatorial coordinate determined at the center epoch for each of the three date segments. The values in parentheses indicate uncertainties in the unit of the last quoted digit.

Data span (MJD)	Epoch (MJD)	RA (h:m:s)	DEC (° :′ :″)
51560–55199	53361	17:05:36.031(3)	−19:06:39.3(3)
55199–55953	55573	17:05:35.9969(14)	−19:06:39.51(16)
55953–56741	56350	17:05:35.9851(18)	−19:06:39.42(12)

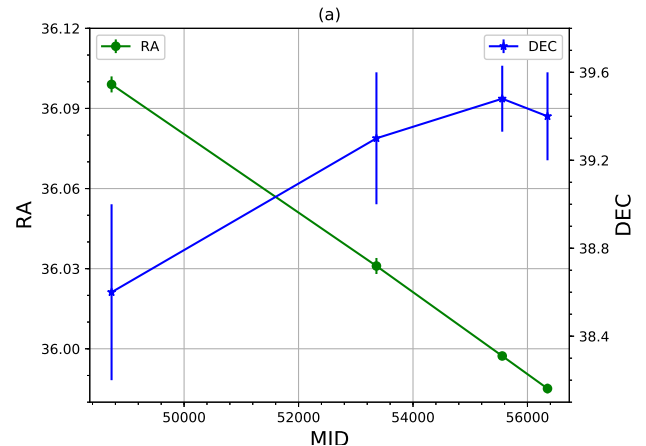


Fig. 2 Change of the right ascension and declination along with epoch.

²<http://www.atnf.csiro.au/research/pulsar/psrcat/>

As the two glitches occurred around MJD 55199 and MJD 55953 (detail are given in subsequent analysis), the timing data is divided into three segments to obtain position and proper motion more accurately. The two glitches are not obvious in Figure 1 as they are submerged in the residuals due to the proper motion.

We analyze the position and proper motion of PSR 1705–1906 with the three data segments. The first segment (between MJD 51560 to MJD 55199) has significant red noise after fitting for the position, spin frequency, frequency derivative and second derivative of the frequency. It is always a challenge to whiten the timing residuals when the data is dominated by red noise, which is a well-known problem to pulsar observers. To deal with it usually involve subtracting a high order polynomial or harmonically related sinusoids when carrying out the least squares fit. Coles et al. (2011) have shown that such technique is not optimal and often leads to a severe underestimation of the parameter error, and so proposed a prewhitening method known as the Cholesky method. The Cholesky solution uses a linear transformation, which is derived from the covariance matrix of the residuals, to pre-whiten the residuals. It estimates an analytic model for the low frequency component of the spectrum for the timing noise (see Section 4.1 for details). We fit the pulsar parameters (including the position and proper motion) with the analytic red noise model, and obtained the right ascension $\alpha=17:05:36.031(3)$ and declination $\delta = -19:06:39.3(3)$ at MJD 53361 in equatorial coordinates as shown in Table 3. These values will be adopted in the subsequent analysis. As the data in the last two segments are not found to have non-white noise after fitting the position, ν , $\dot{\nu}$, and $\ddot{\nu}$, we employ the polynomial fitting for the high-order derivatives of the spin frequency, not the Cholesky method, to estimate the positions. Table 3 shows positions at the center epoch for each of three segments in equatorial coordinates.

We plot the positions of the pulsar in the four epochs in Figure 2 to better show the changes of position. The first position in MJD 48733 (21 April 1992) is obtained from the paper by Hobbs et al. (2004). In this work, we found that the uncertainties for the position of PSR J1705–1906 in declination is greater than that in right ascension. The reason is that the pulsar is subjected to strong roemer delay and shapiro delay if it lies in or very close to the ecliptic plane. Therefore, the predicted positions and proper motions in ecliptic latitude are relatively poor, nor can we precisely measure its position and proper motion in declination, as the angle between the equator and the ecliptic is small of ~ 23.5 degrees.

Proper motion of the pulsar is calculated using

$$\mu_\alpha = \dot{\alpha} \cos \delta \quad \mu_\delta = \dot{\delta}, \quad (3)$$

$$\mu_{tot} = (\mu_\alpha^2 + \mu_\delta^2)^{\frac{1}{2}}, \quad (4)$$

where μ_α is proper motion in right ascension, μ_δ is proper motion in declination and μ_{tot} is total proper motion in two dimensions. We derive the proper motion using the positions obtained from the first segment and Hobbs et al. (2004). The results are $\mu_\alpha = -76(5) \text{ mas yr}^{-1}$ and $\mu_\delta = -55(39) \text{ mas yr}^{-1}$, which are consistent with the measurements of $\mu_\alpha = -78(9) \text{ mas yr}^{-1}$ and $\mu_\delta = -116(82) \text{ mas yr}^{-1}$ given by Hobbs et al. (2004). Our results have smaller uncertainties as they are derived from a longer data span.

3.2 Distance and velocity

Distance and transverse velocity of the pulsar determine the luminosity of the source and its location in the Galaxy, all of which are important for research of the origin, evolution and emission properties of the object in question. The distribution of free electrons in the Galaxy, the Magellanic Clouds and the intergalactic medium can be used to estimate distance to a pulsar based on its dispersion measure. We calculated the distance to PSR J1705–1906 using the latest electronic density model YMW16 (Yao et al. 2017) and the dispersion measurement (DM) of $22.907(3) \text{ pc cm}^{-3}$ (Hobbs et al. 2004). A distance of 0.7469 kpc is obtained from YMW16, which is smaller than 0.89 kpc predicted by NE2001. We note that 68% of the distances predicted by YMW16 will have a relative uncertainty of less than 0.4. The pulsar transverse velocity is determined with $V_T = 4.74 \mu_{tot} D \approx 304(57) \text{ km s}^{-1}$, where D is distance (in kpc) and the uncertainty in μ_{tot} is dominated by the error in proper motion and distance. Lyne and Lorimer (1994) have demonstrated that the average transverse velocity of pulsars is $V_T = 300(30) \text{ km} \cdot \text{s}^{-1}$ based on analysis of proper motions and distances from a large number of pulsars. It seems that PSR J1705–1906 has a medial transverse velocity among pulsars.

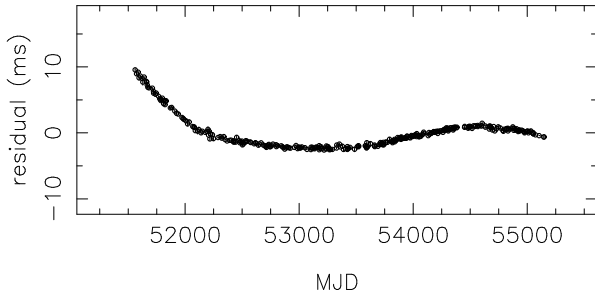
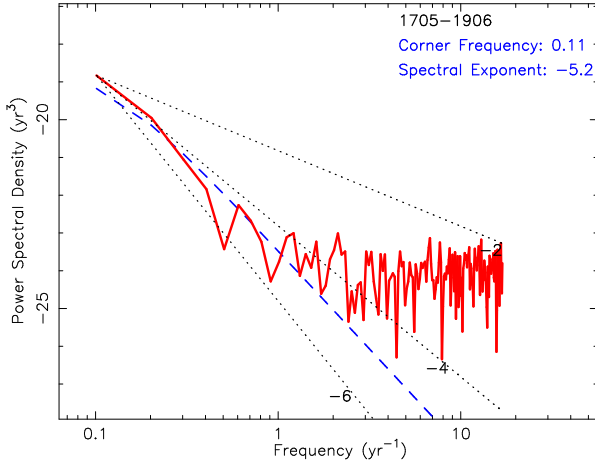
4 Timing irregularities

4.1 Timing noise

Figure 3 shows the pre-glitch timing residuals with respect to a solution that contains the ν and $\dot{\nu}$ for PSR J1705–1906. It is clear that pre-glitch timing

Table 4 The Δ_8 values of PSR J 1705–1906.

Data span (MJD)	ν (s^{-1})	$\ddot{\nu}$ (10^{-26} s^{-3})	Δ_8
51560–52764	3.344608546886(8)	12(3)	−2.17(11)
52764–53968	3.344603712604(5)	4(2)	−2.65(22)
53968–55199	3.344598894692(4)	3(1)	−2.77(14)

**Fig. 3** The timing residuals of PSR J1705–1906 between MJD 51560 and MJD 55199.**Fig. 4** The observed power spectra of the pre-glitch timing noise for PSR J1705–1906. The red solid line is the observed spectral noise, the blue dashed line represents the red noise model. The dotted lines show power spectra with exponent of -2 , -4 and -6 from top to bottom, respectively.

residuals exhibit significant red noise. In order to characterize the stability of the pulsar and to determine the “amount of timing noise”, we calculate the Δ_8 value (Arzoumanian et al. 1994) given by

$$\Delta_8 = \log\left(\frac{|\ddot{\nu}|}{6\nu}t^3\right), \quad (5)$$

where ν and $\ddot{\nu}$ are measured over a time interval of $t \sim 10^8 \text{ s}$ ($\sim 3 \text{ yr}$). As this pulsar’s pre-glitch data-sets span at least 10 yr, we obtained the Δ_8 values of $-2.17(11)$, $-2.65(22)$, $-2.77(14)$ by fitting ν , $\dot{\nu}$ and $\ddot{\nu}$ to three $\sim 3 \text{ yr}$ segments. Hobbs et al. (2010) confirmed the statistics-averaged correlation between Δ_8 and spin-down rate, \dot{P} , for 366 non-recycled pulsars

$$\Delta_8' = 5.1 + 0.5 \log \dot{P}. \quad (6)$$

With the observed \dot{P} , the inferred value Δ_8' of this pulsar is ~ -2.09 . Table 4 presents the data spans, epochs, the values of ν , $\ddot{\nu}$ and Δ_8 for the three data segments. It is obvious that one of values for Δ_8 (-2.17) is close to the correlation, although the measured ones are scattered.

We use the Cholesky method for the analysis of correlated timing noise. A power-law model, given by

$$P(f) = A[1 + (f/f_c)^2]^{\alpha/2}, \quad (7)$$

can be used to fit the low-frequency noise. Here, A is the amplitude, f_c is the corner frequency and α is the spectral exponent. We estimate f_c and α to match the red spectrum at low frequencies in TEMPO2. For the pre-glitch data, these values are $f_c = 0.11 \text{ yr}^{-1}$ and $\alpha = -5.2$ for a reasonable fit. Figure 4 shows the distribution of power spectra density against frequency. The dotted lines embody the spectral exponent of -2 , -4 , and -6 , which suggest that the noise is dominated by random walk in the phase, ν and $\dot{\nu}$, respectively. The blue dashed line represent the low-frequency model with spectral exponent of ~ -5.2 , indicating that the fluctuations in spin frequency and spin-down rate dominate the red noise. Rotation parameters of $\nu = 3.344603736538(22) \text{ s}^{-1}$, $\dot{\nu} = -4.62782(2) \times 10^{-14} \text{ s}^{-2}$ and $\ddot{\nu} = 4.7(7) \times 10^{-26} \text{ s}^{-3}$ are obtained at MJD 53361 by Cholesky method, which are adopted in the subsequent analysis.

4.2 Glitch

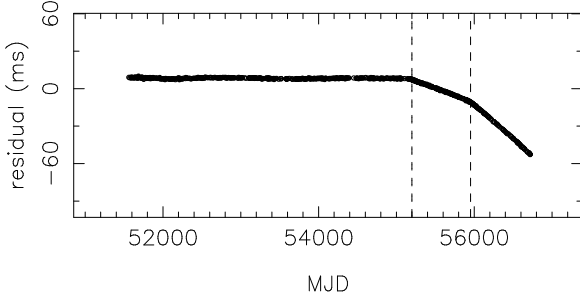
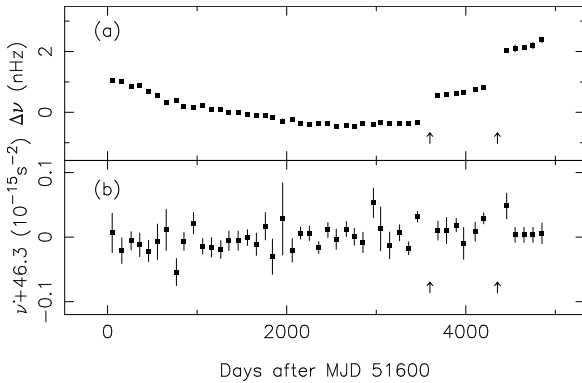
We present the analysis of glitches using Nanshan and Parkes timing data that was collected from 2000 January to 2014 March. The latest astrometric parameters and red noise model are fixed in this analysis. The timing residuals are obtained by comparing the

Table 5 Rotation parameters of PSR J1705–1906 obtained from different segments.

Data span	Epoch (MJD)	ν (s^{-1})	$\dot{\nu}$ ($\times 10^{-14} \text{ s}^{-2}$)	$\ddot{\nu}$ ($\times 10^{-26} \text{ s}^{-3}$)	No. of TOAs	post-fit Rms (μs)
51561 - 55199	53361	3.344603736531(1)	-4.627826(2)	5.01(5)	344	115.994
55199 - 55953	55573	3.344594893724(7)	-4.62664(3)	1.9(6)	130	70.102
55953 - 56741	56350	3.344591788845(5)	-4.62611(5)	1.9(8)	95	168.725

Table 6 Glitch parameters for PSR J1705–1906.

Data span	Epoch (MJD)	Extrapolated		Fitted		No. of TOAs	post-fit Rms (μs)
		$\Delta\nu_{\text{g}}/\nu$ ($\times 10^{-9}$)	$\Delta\dot{\nu}_{\text{g}}/\dot{\nu}$ ($\times 10^{-3}$)	$\Delta\nu_{\text{g}}/\nu$ ($\times 10^{-9}$)	$\Delta\dot{\nu}_{\text{g}}/\dot{\nu}$ ($\times 10^{-3}$)		
51560–55372	55199	0.26(1)	0.4(4)	0.29(5)	0.3(5)	378	140.156
55199–56153	55953	0.28(2)	0.2(1)	0.27(1)	0.5(2)	159	68.512

**Fig. 5** The timing residuals of PSR J1705–1906 after updating the latest astrometry parameters and spin parameters.**Fig. 6** Variations of the spin-frequency residuals ν showing two glitches that occurred around MJD 55199 and MJD 55953

observed ToAs with the predicted ToAs given by Equation 1. It was not possible to obtain a white residual or a smooth timing residual for PSR J1705–1906 for the whole data set, because the timing observations showed that PSR J1705–1906 underwent two small glitches, as indicated in Figure 5. To investigate the spin behavior of PSR J1705–1906, ν and $\dot{\nu}$ are obtained from independent fitting for short section of data, each of which typically spans ~ 100 d with overlapping of ~ 50 d. Figure 6 presents the variations of spin parameters after subtracting the pre-glitch timing model. Two small glitches are visible which occurred with jumps in spin frequency of $\Delta\nu \sim 0.9 \times 10^{-9}$ Hz and $\sim 1.0 \times 10^{-9}$ Hz, respectively. Comparing with the spin-frequency in post-glitches for PSR J1705–1906, the observations do not appear to have any relaxation. Yu et al. (2013) also observed similar phenomenon in PSR J0834–4159, PSR J1413–6164, PSR J1801–2304. In our case, the jump parameters obtained from the observations are likely permanent or long-term values.

If the gap between observations around a glitch is not too large, the glitch epoch can be estimated more accurately by requiring a phase-connected solution over the gap in the TEMPO2 fit. However, if the gap is too large, the glitch epoch is estimated from the ToA at the mid-point of the last pre-glitch and the first post-glitch, with the quoted uncertainty covers the gap in the data. For PSR 1705–1906, as the gap between observations around the glitch is too large, the estimated epochs for the two glitches are MJD 55199(6) (2010 01 03) and MJD 55953(16) (2012 01 27).

With the epochs fixed, the pre- and the post-glitch spin parameters given by Table 5 can be determined. We extrapolate the spin parameters to the glitch epochs and calculate the fraction jump in ν and $\dot{\nu}$. The results are given in the third and fourth columns in Table 6.

The fifth and sixth columns give the results for the glitch parameters from directly fitting in TEMPO2. The values of glitch parameters are $\Delta\nu_g/\nu = 0.29(5) \times 10^{-9}$ and $\Delta\dot{\nu}_g/\dot{\nu} = 0.3(5) \times 10^{-3}$ around MJD 55199, and $\Delta\nu_g/\nu = 0.27(1) \times 10^{-9}$ and $\Delta\dot{\nu}_g/\dot{\nu} = 0.5(2) \times 10^{-3}$ around MJD 55953, respectively. We find that the parameter values and their corresponding uncertainties obtained from extrapolation and fitting **are consistent**.

5 pulse profiles of PSR J1705–1906

Figure 7 shows the pulse profile of PSR J1705–1906 obtained at 1540 MHz using the Nanshan 25-m radio telescope. The pulse profile consists of a main pulse and an interpulse, with separation of ~ 0.5 phase from each other. The main pulse contains two components with the intensity in the trailing component lower than that of the leading component by about **20%**. The W_{50} and W_{10} are given by 0.009 s and 0.014 s, which correspond to 3% and 4.7% of the pulse period, respectively, where W_{50} and W_{10} are the full width at the 50% and 10% levels of pulse peak, respectively. The interpulse has a fraction intensity of ~ 0.43 , weaker than the half-peak intensity of the main pulse. It is obvious from Figure 7 that the width of the interpulse is less than that of the main pulse.

Changes in pulse profile in association with glitches have been reported for several pulsars such as PSR J0742–2822 (Keith et al. 2013), 1119–6227 (Weltevred et al. 2013) and 2037+3621 (Kou et al. 2018). In order to investigate whether such a link also exists in PSR J1705–1906, we carefully examined the average pulse profile in the pre- and post-glitch data collected from Nanshan at 1540 MHz. Figure 8 shows the normalized average pulse profile from three different time segments with the pulse phase aligned. We found that the pulse width and the separation between main pulse and interpulse remain unchange between pre- and post-glitch.

6 Discussion and conclusions

In this paper we have

1. updated the position, proper motion, distance and velocity of PSR J1705–1906 in the equatorial coordinates;
2. calculated the Δ_8 value, which allowed the assessment of the size of the timing noise, and obtained a better timing red noise model using Cholesky solution;

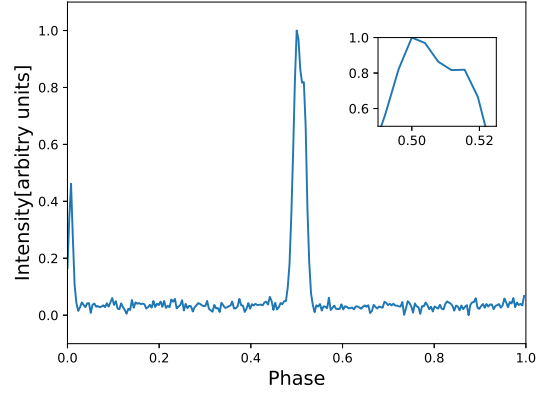


Fig. 7 The pulse profile of PSR 1705–1906 at 1540 MHz obtained **using** Nanshan 25-m radio telescope.

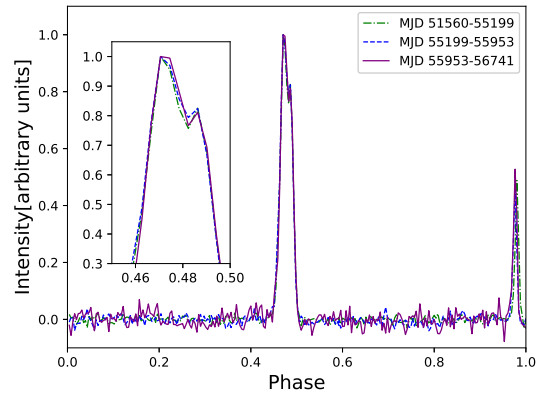


Fig. 8 The pulse profiles of PSR 1705–1906 from three different time segments obtained using Nanshan 25-m radio telescope at 1540 MHz.

Table 7 The glitch size of pulsars with similar characteristic age and spin parameters to PSR J1705–1906.

PSR	P (s)	\dot{P} ($\times 10^{-15} \text{ s}^{-1}$)	τ_c ($\times 10^6 \text{ yr}$)	Epoch (MJD)	$\Delta\nu_g/\nu$ ($\times 10^{-9}$)	References
J0611+1436	0.27033	3.997	1.07	55818	5575.3	Lyne et al. (2017)
J1705–1906	0.29899	4.1379	1.14	48902	0.4(1)	Espinoza et al. (2011)
				55199	0.29(5)	this work
				55953	0.27(1)	this work
J1812–1718	1.20537	19.077	1.0	49932(1)	1.5(2)	Espinoza et al. (2011)
				53106.2(1)	14.8(2)	Espinoza et al. (2011)
				54365.8(3)	1.4(1)	Espinoza et al. (2011)
J1902+0615	0.67350	7.713	1.38	48653.7(1)	0.4(1)	Espinoza et al. (2011)
				49447(1)	0.3(1)	Espinoza et al. (2011)
				50316(2)	0.3(1)	Espinoza et al. (2011)
				51136(4)	0.4(1)	Espinoza et al. (2011)
				54239(1)	0.26(3)	Espinoza et al. (2011)
J2225+6535	0.68254	9.661	1.12	43072(40)	1707(1)	Backus et al. (1982)
				51900	0.14(3)	Janssen and Stappers (2006)
				52950	0.08(4)	Janssen and Stappers (2006)
				53434(13)	0.2(1)	Janssen and Stappers (2006)
				54266(14)	0.36(8)	Janssen and Stappers (2006)
J2257+5909	0.36824	5.753	1.01	49488.2(2)	0.75(4)	Espinoza et al. (2011)
J1818–1422	0.29149	2.036	2.27	52057(7)	0.54(5)	Yuan et al. (2010)
J1957+2831	0.30768	3.11	1.57	52485(3)	0.3(1)	Espinoza et al. (2011)
				52912(3)	0.13(3)	Espinoza et al. (2011)
				54692.8(3)	5.8(3)	Espinoza et al. (2011)

3. identified two new glitches and obtained their parameters.

The new two glitches from PSR J1705–1906 are quite small and do not appear to have significant relaxation, and have amplitudes similar to the 1992 event. In our case, the jumps obtained from the observations are permanent or long-term values. If we assume the pulsar glitched three times since it was discovered, then using the glitch activity parameter, which is defined as

$$A_g = \frac{1}{T} \sum \frac{\Delta\nu_g}{\nu}, \quad (8)$$

where T is the total data span (McKenna and Lyne 1990), a value of $A_g \sim 2.0 \times 10^{-11} \text{ yr}^{-1}$ is obtained. This is consistent with the assumption that relatively old pulsars have low glitch activity (A_g) due to small and rare glitches (Espinoza et al. 2011; Hobbs et al. 2010; Lyne et al. 2000; Yuan et al. 2010). A correlation is reported between the mean glitch rate and spin down rate with $\langle \dot{N}_g \rangle \propto |\dot{\nu}|^{0.47(4)}$ (Espinoza et al. 2011) suggesting that pulsars with low spin-down rates tend to exhibit small glitches. It is noted that this correlation is based on a large sample, which includes those pulsars that are yet to be detected with glitches. For PSR J1705–1906 with $|\dot{\nu}| \sim 46.288 \times 10^{-15} \text{ s}^{-2}$, the

predicted $\langle \dot{N}_g \rangle$ is $\sim 0.019(2) \text{ yr}^{-1}$. The observed mean glitch rate is large with a value of $\sim 0.083 \text{ yr}^{-1}$, which is about 4.4 times that of the predicted value. This suggests that, in term of glitch, PSR J1705–1906 is more active than those pulsars with similar spin down rate.

For radio pulsars with characteristic age in the range between 1.0×10^6 and $1.4 \times 10^6 \text{ yr}$, a total of 18 glitches³ were identified in six pulsars including PSR J1705–1906, of which four pulsars (PSRs J1705–1906, J1812–1718, J1902+0615, J2225+6535) have each at least three glitches detected (**Backus et al. 1982; Janssen and Stappers 2006; Espinoza et al. 2011**).

For those radio pulsars with similar period (from 0.29 s to 0.31 s) and similar \dot{P} in the range between 2.0×10^{-15} and $6 \times 10^{-15} \text{ s s}^{-1}$, at least four glitches were identified in two pulsars, PSRs J1818–1422 and J1957+2831 (Yuan et al. 2010; Espinoza et al. 2011). The glitch sizes of these pulsars with similar characteristic age and spin parameters are given in Table 7. Almost all of these glitches have size of $\sim 10^{-9}$, except for the glitches in PSRs J0611+1436 and J2225+6535, which have sizes in the order of $\sim 10^{-6}$ (**Backus et al. 1982; Lyne et al. 2017**). At this stage, we cannot exclude

³<http://www.atnf.csiro.au/people/pulsar/psrcat/glitchTbl.html>

the possibility of occurrence of large glitch in PSR J1705–1906, and so a continuous monitoring of the pulsar is worthwhile.

Pulsar glitch is one of the very few instances through which we can study the interior of a neutron star and the properties of matter at supernuclear density. Glitches have been argued to be the result of either starquakes or from angular momentum exchange between the faster rotating interior superfluid and the solid crust (Haskell and Melatos 2015). Consider the starquake regime, we infer that the fractional change in the radius of this pulsar due to the two glitches is $\Delta r/r \sim 0.28(3) \times 10^{-9}$ and the fractional change in moment of inertia is $\Delta I/I \sim -0.56(6) \times 10^{-9}$. In the angular momentum exchange model, the interior vortices migrate outward and transfer momentum to the crust causing the crust to spin up and resulting in a glitch. Eya et al. (2017) introduce the fractional moment of inertia (FMI), which estimates the fraction of neutron star components involved in the glitch process,

$$\frac{I_{res}}{I_c} = - \sum_1^n \frac{1}{\dot{\nu}_c} \frac{\Delta \nu_i}{t_i}, \quad (9)$$

where I_{res} is moment of inertia of the momentum reservoir, t_i is the time interval preceding the i th glitch, $\dot{\nu}_c$ is the spin frequency derivatives of the crust and I_c is the moment of inertia of the solid crust and all other components (superfluid interior and/or core) that strongly coupled to it. The FMI for 26 frequently glitching pulsars ranges from 1.0×10^{-6} to 1.8 with a mean value of 10^{-3} and a distribution of the FMI that resembles a normal distribution with peak at 10^{-2} . We obtained $I_{res}/I \approx 3.37 \times 10^{-4}$ for PSR J1705–1906, which is consistent with the correlation between the fraction glitch size and the fractional moment of inertia (Eya et al. 2017).

Acknowledgements

This work is supported by West light Foundation of CAS, Grant No. XBBS201421; Strategic Priority Research Programme of Chinese Academy of Sciences, Grant No. XDB23010200; and National Natural Science Foundation of China (NSFC No. U1531137, 11373011). The FAST Fellowship is supported by Special Funding for Advanced Users, budgeted and administrated by Center for Astronomical Mega-Science, Chinese Academy of Sciences (CAMS). JBW acknowledges support from NSFC, Grant 11403086, U1431107, 11573059). NW is supported by National Basic Research Program of China (2015CB857100), the National Program on Key Research and Development Project,

Grant No. 2016YFA0400804. RY acknowledges supports from NSFC Project no. 11573059, and the West Light Foundation of the Chinese Academy of Sciences, project 2016-QNXZ-B-24.

This work is based on observations made with the Urumqi Nanshan 25 m Telescope, which is operated by XAO and the Key Laboratory of Radio Astronomy, Chinese Academy of Sciences. The Parkes radio telescope is part of the Australia Telescope, which is funded by the Commonwealth of Australia for operation as a National Facility managed by the Commonwealth Scientific and Industrial Research Organization.

References

- Arzoumanian, Z., Nice, D.J., Taylor, J.H., Thorsett, S.E.: *Astrophys. J.* **422**, 671 (1994)
- Backus, P.R., Taylor, J.H., Damashek, M.: *Astrophys. J. Lett.* **255**, 63 (1982)
- Briskin, W.F., Benson, J.M., Goss, W.M., Thorsett, S.E.: Very long baseline array measurement of nine pulsar parallaxes **571**, 906 (2002)
- Briskin, W.F., Fruchter, A.S., Goss, W.M., Herrnstein, R.S., Thorsett, S.E.: Proper-motion measurements with the VLA. II. Observations of twenty-eight pulsars **126**, 3090 (2003)
- Coles, W., Hobbs, G., Champion, D.J., Manchester, R.N., Verbiest, J.P.W.: *Mon. Not. R. Astron. Soc.* **418**, 561 (2011)
- D'Alessandro, F.: *Astrophys. Space Sci.* **246**, 73 (1996)
- Deller, A.T., Vigeland, S.J., Kaplan, D.L., Goss, W.M., Briskin, W.F., Chatterjee, S., Cordes, J.M., Janssen, G.H., Lazio, T.J.W., Petrov, L., Stappers, B.W., Lyne, A.: *Astrophys. J.* **828**, 8 (2016)
- Du, Y., Yang, J., Campbell, R.M., Janssen, G., Stappers, B., Chen, D.: *Astrophys. J. Lett.* **782**, 38 (2014)
- Edwards, R.T., Hobbs, G.B., Manchester, R.N.: *Mon. Not. R. Astron. Soc.* **372**, 1549 (2006)
- Espinoza, C.M., Lyne, A.G., Stappers, B.W., Kramer, M.: *Mon. Not. R. Astron. Soc.* **414**, 1679 (2011)
- Eya, I.O., Urama, J.O., Chukwude, A.E.: *Astrophys. J.* **840**, 56 (2017)
- Gunn, J.E., Ostriker, J.P.: *Astrophys. J.* **160**, 979 (1970)
- Haskell, B., Melatos, A.: *International Journal of Modern Physics D* **24**, 1530008 (2015)
- Hobbs, G., Lyne, A.G., Kramer, M.: *Mon. Not. R. Astron. Soc.* **402**, 1027 (2010)
- Hobbs, G.B., Edwards, R.T., Manchester, R.N.: *Mon. Not. R. Astron. Soc.* **369**, 655 (2006)
- Hobbs, G., Lyne, A.G., Kramer, M., Martin, C.E., Jordan, C.: *Mon. Not. R. Astron. Soc.* **353**, 1311 (2004)
- Hobbs, G., Lorimer, D.R., Lyne, A.G., Kramer, M.: *Mon. Not. R. Astron. Soc.* **360**, 974 (2005)
- Hobbs, G., Miller, D., Manchester, R.N., Dempsey, J., Chapman, J.M., Khoo, J., Applegate, J., Bailes, M., Bhat, N.D.R., Bridle, R., Borg, A., Brown, A., Burnett, C., Camilo, F., Cattalini, C., Chaudhary, A., Chen, R., D'Amico, N., Kedziora-Chudczer, L., Cornwell, T., George, R., Hampson, G., Hepburn, M., Jameson, A., Keith, M., Kelly, T., Kosmynin, A., Lenc, E., Lorimer, D., Love, C., Lyne, A., McIntyre, V., Morrissey, J., Pienaar, M., Reynolds, J., Ryder, G., Sarkissian, J., Stevenson, A., Treloar, A., van Straten, W., Whiting, M., Wilson, G.: *Proc. Astron. Soc. Aust.* **28**, 202 (2011)
- Hotan, A.W., van Straten, W., Manchester, R.N.: *Proc. Astron. Soc. Aust.* **21**, 302 (2004)
- Hou, X., Smith, D.A., Guillemot, L., Cheung, C.C., Cognard, I., Craig, H.A., Espinoza, C.M., Johnston, S., Kramer, M., Reimer, O., Reposeur, T., Shannon, R., Stappers, B.W., Weltevrede, P.: *Astron. Astrophys.* **570**, 44 (2014)
- Janssen, G.H., Stappers, B.W.: *Astron. Astrophys.* **457**, 611 (2006)
- Keith, M., Shannon, R.M., S, J.: *Mon. Not. R. Astron. Soc.* **432**, 3080 (2013)
- Kou, F.F., Yuan, J.P., Wang, N., Yan, W.M., Dang, S.J.: *arxiv:1801.01248* (2018)
- Lai, D., Qian, Y.-Z.: *Astrophys. J.* **505**, 844 (1998)
- Lai, D., Chernoff, D.F., Cordes, J.M.: *Astrophys. J.* **549**, 1111 (2001)
- Li, L., Wang, N., Yuan, J.P., Wang, J.B., Hobbs, G., Lentati, L., Manchester, R.N.: *Mon. Not. R. Astron. Soc.* **460**, 4011 (2016)
- Lyne, A.G., Lorimer, D.R.: *Nature* **369**, 127 (1994)
- Lyne, A.G., Shemar, S.L., Smith, F.G.: *Mon. Not. R. Astron. Soc.* **315**, 534 (2000)
- Lyne, A.G., Stappers, B.W., Bogdanov, S., Ferdman, R.D., Freire, P.C.C., Kaspi, V.M., Knispel, B., Lynch, R., Allen, B., Brazier, A., Camilo, F., Cardoso, F., Chatterjee, S., Cordes, J.M., Crawford, F., Deneva, J.S., Hessels, J.W.T., Jenet, F.A., Lazarus, P., van Leeuwen, J., Lorimer, D.R., Madsen, E., McKee, J., McLaughlin, M.A., Parent, E., Patel, C., Ransom, S.M., Scholz, P., Seymour, A., Siemens, X., Spitler, L.G., Stairs, I.H., Stovall, K., Swiggum, J., Wharton, R.S., Zhu, W.W., Aulbert, C., Bock, O., Eggenstein, H.-B., Fehrmann, H., Machenschalk, B.: *Astrophys. J.* **834**, 137 (2017). 1608.09007
- Manchester, R.N., Taylor, J.H., Van, Y.Y.: *Astrophys. J. Lett.* **189**, 119 (1974)
- Manchester, R.N., Lyne, A.G., Taylor, J.H., Durdin, J.M., Large, M.I., Little, A.G.: The Second Molonglo Pulsar Survey – Discovery of 155 Pulsars **185**, 409 (1978)
- McKenna, J., Lyne, A.G.: *Nature* **343**, 349 (1990)
- Ng, C.-Y., Romani, R.W.: *Astrophys. J.* **644**, 445 (2006)
- Wang, N., Manchester, R.N., Zhang, J., Wu, X.J., Yusup, A., Lyne, A.G., Cheng, K.S., Chen, M.Z.: *Mon. Not. R. Astron. Soc.* **328**, 855 (2001)
- Weltevrede, P., Johnston, S., Espinoza, C.M.: *Mon. Not. R. Astron. Soc.* **432**, 3080 (2013)
- Yan, Z., Shen, Z.-Q., Yuan, J.-P., Wang, N., Rottmann, H., Alef, W.: *Mon. Not. R. Astron. Soc.* **433**, 162 (2013)
- Yao, J.M., Manchester, R.N., Wang, N.: *Astrophys. J.* **835**, 29 (2017)
- Yu, M., Manchester, R.N., Hobbs, G., Johnston, S., Kaspi, V.M., Keith, M., Lyne, A.G., Qiao, G.J., Ravi, V., Sarkissian, J.M., Shannon, R., Xu, R.X.: *Mon. Not. R. Astron. Soc.* **429**, 688 (2013)
- Yuan, J.P., Wang, N., Manchester, R.N., Liu, Z.Y.: *Mon. Not. R. Astron. Soc.* **404**, 289 (2010)